Climate change in a conceptual atmosphere–plankton model

György Károly[1], Rudolf Dániel Prokaj[2], István Scheuring[3], and Tamás Tél[4]

[1]Budapest University of Technology and Economics, Institute of Nuclear Techniques, Műegyetem rkp. 3., 1111 Budapest, Hungary
[2]Budapest University of Technology and Economics, Department of Stochastics, Műegyetem rkp. 3., 1111 Budapest, Hungary
[3]MTA-ELTE Theoretical Biology and Evolutionray Ecology Research Group, Department of Plant Taxonomy, Ecology and Theoretical Biology, Eötvös University, Budapest, Hungary and MTA Centre for Ecological Research, Evolutionary Systems Research Group, Tihany, Hungary
[4]Department of Theoretical Physics, Eötvös University, Budapest, Hungary, and MTA-ELTE Theoretical Physics Research Group, Budapest, Hungary

Correspondence: György Károlyi (karolyi@reak.bme.hu)

Abstract. We develop a conceptual coupled atmosphere-phytoplankton model by combining the Lorenz'84 general circulation model and the logistic population growth model under the condition of a climate change due to a linear time dependence of the strength of anthropogenic atmospheric forcing. The following types of couplings are taken into account: a) the temperature modifies the total biomass of phytoplankton via the carrying capacity, b) the extraction of carbon dioxide by phytoplankton
5 slows down the speed of climate change, c) the strength of mixing/turbulence in the oceanic mixing layer is in correlation with phytoplankton productivity. We carry out an ensemble approach (in the spirit of the theory of snapshot attractors) and concentrate on the trends of the average phytoplankton concentration and average temperature contrast between the pole and equator, forcing the atmospheric dynamics. The effect of turbulence is found to have the strongest influence on these trends. Our results show that a) sufficiently strong mixing is able to force the typical phytoplankton concentration to always decay
10 globally in time, and the temperature contrast to decrease faster than what follows from direct anthropogenic influences. Simple relations found for the trends without this coupling do, however, remain valid, just the coefficients become dependent on the strength of coupling with oceanic mixing. In particular, the phytoplankton concentration and its coupling to climate is found to modify the trend of global warming, and is able to make it stronger than what it would be without biomass.

15 ## 1 Introduction

Large scale general circulation models, in general, take into account the interaction of the atmosphere with land vegetation and marine biomass production in the form of a huge number of parametrized processes (see e.g. Marinov et al, 2010; Zhong et al, 2011; Mongwe et al, 2018; Wilson et al, 2018). A basic understanding of such coupling is, however, easier to obtain in low

order conceptual models, where even analytic results may be available. Probably the most important component that needs to
20 be included in such conceptual models is the phytoplankton content of the ocean.

Oceans are the major sink for the atmospheric CO_2 (Hader et al, 2014; Li et al, 2012). CO_2 is either stored as dissolved
inorganic carbon or transferred to the underlying sediment by biological carbon pump. The motor of the biological pump is
phytoplankton which is one of the major components of the global carbon cycle hence influencing decisively atmoshperic CO_2
(Hutchins and Fu, 2017; Sanders et al, 2014; Turner, 2015; Falkowski et al, 2000). Besides, phytoplankton is resonsible for
25 nearly half of the total primary production on Earth (Basu and Mackey, 2018). Consequently, it is extremely important to un-
derstand the intercation of primary production in oceans with effects contributing to global climate change. However, the task
is very challanging: change in atmospheric CO_2 level can have opposite impact on processes influencing the phytoplankton
and the intensity of the biological carbon pump. Increased atmospheric CO_2 level increases ocean temperature, decreases pH,
increases water stratification, inflences general oceanic circulation. These can all modify the net productivity and the compo-
30 sition of phytoplankton, and can have either positive or negative net effect on the biological carbon pump (Basu and Mackey,
2018, and references therein).

In accordance with the current trend to include biogeochemistry in climate models (see e.g. Schlunegger et al, 2019), we
consider a simple conceptual model, where increasing the global temperature affects the global primary production of ocean. As
phytoplankton plays significant role in the global CO_2 balance (De La Rocha and Passow, 2014; Falkowski, 2014; Guidi et al,
35 2016), our aim is to take an elementary description of phytoplankton dynamics coupled to an elementary model of the atmo-
sphere. Because of the ambiguity in the direct and indirect effects of increased CO_2 concentration on phytplankton dynamics
and biological carbon pump, we study scenarios when climate change either stimulates or inhibits phytoplankton production.
As atmospheric model, we use Lorenz' elementary global circulation model (Lorenz, 1984), which was extended to mimic cli-
mate change (Drótos et al, 2015). The global phytoplankton concentration is represented by a simple logistic model in which
40 the carrying capacity is coupled with the CO_2 content depending also on the concentration itself and on the wind energy
influencing the oceanic mixing layer.

An appropriate treatment of even elementary models describing climate change is not obvious since basic parameters change
with time and, therefore, traditional long-time averages cannot be used to define (in the sense of any statistical quantifiers) a
state of the climate. An emerging new view, already embraced by Drótos et al (2015), follows a different route to obtain
45 information on instantaneous statistical quantifiers (e.g. expected, average properties) of the climate. Since our information
on the actual state of the climate is incomplete, one imagines an ensemble of parallel Earth systems carrying parallel climate
realizations subjected to the *same set of physical laws*, boundary conditions and external forcing, but with *different initial
conditions*. Then the chaotic or turbulence-like properties of the climate dynamics allows for distinct climate realizations.
These realizations, however, cannot be arbitrary since only those are permitted that are compatible with physical laws and the
50 given forcing. The ensemble of realizations defines a probability distribution of all the relevant variables at *any instant of time*
from which one can obtain expected, ensemble average properties of the climate.

The mathematical concepts underlying this qualitative view are snapshot (Romeiras et al, 1990) or pullback (Ghil et al, 2008)
attractors. One might consider the ensemble of all permitted climate realizations over all times as the pullback attractor of the

problem, and the set of the permitted states of the climate at a given time instant as the snapshot attractor belonging to that
time instant (their union over all time instants is the pullback attractor). Both views express that the climate system possesses
a plethora of possibilities. In the terminology of climate science, climate has a strong internal variability (e.g.Stocker et al
(2013)). The concept of snapshot or pullback attractors is nothing but a reformulation of this fact in dynamical terms.

In numerical simulations, we consider the members of an ensemble simulation to describe parallel climate realizations
only after the initial conditions are "forgotten", transient dynamics disappears. Due to dissipation, this time is typically
short compared to the time span of interest. Such an ensemble approach has been applied, besides low order climate mod-
els (Chekroun et al, 2011; Bódai et al, 2011; Bódai and Tél, 2012; Bódai et al, 2013; Drótos et al, 2015), to general circulation
models (Haszpra and Herein, 2019; Kaszás et al, 2019; Pierini et al, 2018, 2016; Drótos et al, 2017; Herein et al, 2017, 2019;
Haszpra et al, 2019) and also to experimental situations (Vincze, 2016; Vincze et al, 2017).

The ensemble approach in our conceptual model corresponds to generating parallel atmosphere–phytoplankton realizations
from different initial conditions. In our model, the number of variables is 4, hence the snapshot attractor in the full state space
is difficult to visualize. We therefore concentrate on ensemble averages, and the internal variability will be expressed in terms
of variances. We include, in a simple, heuristic form, *important feedbacks* in the model: a) the change in the atmospheric
temperature modifies phytoplankton concentration, b) the extraction of CO_2 by phytoplankton, and c) wind energy enhances
the strength of turbulence in the oceanic mixing layer which increases the phytoplankton production (Estrada and Berdalet,
1997; Peters and Marrasé, 2000; Jäger et al, 2010).

The paper is organized as follows. In section 2 we describe the model and define the relevant coupling parameters. Without
mixing, exact relations can be derived, the most important of these are summarized in Section 3, while details of the calculations
are relegated to Supplementary Material I. In the presence of mixing, numerical simulations are carried out in the spirit of
snapshot attractors. The results are summarized in Section 4 where one learns that the extraction effect of CO_2 has the least
influence on the general behavior in the presence of mixing. The feedback of the temperature contrast on the phytoplankton
concentration has important consequences, but these are suppressed by a sufficiently strong mixing, which converts the typical
phytoplankton concentration to always decay in time, and surprisingly, the typical temperature contrast is found to decrease
faster than that solely by direct anthropogenic effects. Planar sections of the 4-dimensional snapshot attractor underlying
the dynamics are presented in Section 5, and our conclusions are drawn in Section 6. Additional figures are presented in
Supplementary Material II.

2 The model

The physical content of Lorenz's atmospheric circulation model for the midlatitudes (Lorenz, 1984, 1990) on one hemisphere
is the following. The main forcing is the temperature difference $T_e - T_p$ between the Equator and the Pole. This is proportional
to model variable F influencing most directly the wind speed of the Westerlies represented by x. As an effect of baroclinic
instability, cyclonic activity facilitates poleward heat transport, two modes of which are represented by y and z. The model

reads as follows:

$$\dot{x} = -y^2 - z^2 - ax + aF(t), \tag{1a}$$

$$\dot{y} = xy - bxz - y + G, \tag{1b}$$

$$\dot{z} = xz + bxy - z. \tag{1c}$$

90 For the parameter setting we take the common choice: $a = 1/4$, $b = 4$, $G = 1$. The equations appear in a dimensionless form with the time unit corresponding to 5 days.

By using time-dependent forcing, $F(t)$, as Drótos et al (2015), we also model the contribution of the varying CO_2 content in association with the greenhouse effect. Besides the variation of CO_2 due to effects appearing in $F(t)$, the extraction of CO_2 by phytoplankton is also included into our model. The CO_2 content stored in marine ecosystems, or buried in the sea

95 bed, is correlated with primary production (Falkowski et al, 1998, 2003). Thus, as discussed in the Introduction, modelling the interaction of phytoplankton and atmospheric dynamics is a good proxy for studying marine ecosystem interaction with atmospheric dynamics. Hence we couple the Lorenzian atmospheric dynamics to that of the photosynthetizing oceanic biomass, assumed to be dominated by phytoplankton of concentration $c(t)$. The temperature contrast parameter thus also depends on the global phytoplankton concentration c: $F(t) \rightarrow F(c(t),t)$, with a form to be given below.

100 Spatial inhomogeneties in nutrient and consequently planton content due to e.g. oceanic eddies and upwellings are known to play an important local role in Nature. However, a global atmospheric model like (1) can adequately be coupled only to a global plankton dynamics model. Therefore, the concentration itself is assumed in this simple set-up to follow a logistic population growth

$$\dot{c} = rc\left(1 - \frac{c}{K(t)}\right). \tag{2}$$

105 Carrying capacity K is taken to depend on the average temperature of the hemisphere, or, equivalently, on the temperature contrast F. As a consequence, K depends on time also via the concentration c: $K(t) = K(c(t),t)$. We shall see that an important oceanic effect, that of the turbulence in the mixing layer, can be incorporated into carrying capacity K, although only on a global scale. Parameter r sets the growth rate of the phytoplankton. If, e.g., $r = 1$, the phytoplankton characteristic time is $5/r = 5$ days, as that of the atmosphere. This latter choice will be kept throughout the paper. The assumption of Eq. (2)

110 for the global phytoplankton dynamics tacitly implies that phytoplanton biomass determines the total biomass of the oceans, and also that no catastrophic events (no mass extinction or invasion of species) can take place in this model.

A basic feature of the observed climate change on Earth is that the polar temperature $T_p(t)$ increases, while the equatorial one T_e remains practically constant (Serezze and Francis, 2006; Blunden and Arndt, 2013). We can thus write in suitable units the temperature contrast parameter as $F(t) = T_e - T_p(t)$. The mean temperature in these units is then $T(t) = (T_e + T_p(t))/2 =$

115 $T_e - F(t)/2$. We are interested in dominant, leading order effects and assume therefore the carrying capacity to be coupled linearly by a small coupling constant to the mean temperature relative to some reference state of mean temperature T_r (in which the temperature contrast parameter is $F_r = 2(T_e - T_r)$). The temperature difference $T - T_r$ is then $-(F - F_r)/2$. We

therefore write

$$K(t) = K_r - \alpha(F(c(t), t) - F_r), \tag{3}$$

120   where K_r is the carrying capacity in the reference state characterized by F_r. Coefficient α represents coupling a) between the carrying capacity K and climate change, represented by F, and shall be called the *enrichment parameter*. This coupling may be either positive or negative. For example, increased CO_2 level enhances the efficiency of photosynthesis ($\alpha > 0$), however, acidification because of increased CO_2 levels depresses respiration ($\alpha < 0$) (Reid et al, 2009; Mackey et al, 2015). Similarly, increased water temperature can have both positive and negative effect on phytoplankton biomass in different regions of Earth

125   (Chust et al, 2014; Roberts et al, 2017). We shall, therefore, allow for both positive and negative values of α with $|\alpha|$ small.

Plankton dynamics influences the temperature contrast. If concentration c increases, the temperature contrast F increases, too, because the biomass extracts more CO_2. In leading order, we therefore express the concentration-dependent temperature contrast parameter as a linear function of the concentration:

$$F(t) = F(c(t), t) = \beta(c(t) - c_r) + F_0(t) \tag{4}$$

130   with a small $\beta > 0$, where c_r is the phytoplankton concentration in the reference state. Coefficient β represents coupling b) due to the extraction of CO_2 by phytoplankton, and we therefore call β the *extraction parameter*. The second term, $F_0(t)$, represents the primary external forcing due to the CO_2 content of anthropogenic origin. The increase of both F_0 and $(c(t) - c_r)$ leads to an increase in the temperature contrast $F(t)$. With this form of F the carrying capacity (3) is

$$K(t) = K_r - \alpha[\beta(c(t) - c_r) + F_0(t) - F_r]. \tag{5}$$

135   Without a restriction of generality, we can choose the reference carrying capacity to be $K_r = 1$, implying a reference concentration $c_r = 1$. This choice only rescales parameters α and β in (3) and (4), respectively.

Starting from negative times, we assume the Earth system to be in climatic and population dynamical equilibrium up to time $t = 0$. This state, chosen as the reference state, is characterized by a time independent mean temperature T_r, concentration $c_r = K_r$, and $F_0(t) = F_r$. At time zero, climate change sets in expressed by a linear decrease in the primary temperature

140   contrast:

$$F_0(t) = F_r - D_0 t, \tag{6}$$

expressing direct anthropogenic effects, with a decrease parameter $D_0 = 2/7300$ for $t > 0$ (Drótos et al, 2015). Since one year corresponds to 73 time units (365 days), $1y = 73$, this form expresses that the temperature contrast decreases by 2 units over 100 years. We shall take $F_r = 9.5$, with which the temperature contrast would go down, after a climate change period of 150

145   years, and without any change in the biomass concentration, to 6.5. We stop the climate change scenario in year 150 because model (1) loses its global chaotic property , which is a prerequisite even for a minimal climate model, for small F.

With this scenario (6) of the anthropogenic influence, the carrying capacity $K(t)$ is, in rescaled units,

$$K(t) = 1 - \alpha[\beta(c(t) - 1) - D_0 t], \tag{7}$$

where $D_0 = 0$ for $t \leq 0$ and $D_0 = 2/7300 = 2.7 \cdot 10^{-4}$ for $t > 0$.

We can model seasonality, too, as Lorenz also did (Lorenz, 1990), by augmenting (6) with a periodic term:

$$F_0(t) = F_r - D_0 t + A \sin(\omega t). \tag{8}$$

His choice was $A = 2$ with $\omega = 2\pi/73$, which we shall adopt. Our climate change starts with year 0, and this year begins at the time instant $t = 0$. Note that this time instant belongs to an autumnal equinox according to (8), and, furthermore, $F_r - D_0 t$ can be considered as the annual mean temperature contrast. Any time $t \bmod 73 = 0$ coincides with other autumnal equinoxes, and results will be presented on this day of the year throughout the paper.

Up to this point, the atmospheric variables have not entered the concentration dynamics. Without the linear and constant terms (representing dissipation and forcing, respectively), Eqs. (1) would conserve the total kinetic energy

$$E = \dot{x}^2 + \dot{y}^2 + \dot{z}^2$$

of the atmosphere. From the point of view of the biomass, it is natural to assume that the activity of the atmosphere influences the ocean dynamics within its uppermost mixing layer (Sverdrup, 1953; Whitt et al, 2017), in particular, the strength of turbulence, and hence the depth of mixing layer. Note that component $\dot{x}^2$ represents the contribution of zonal winds to the total atmospheric energy, while $\dot{y}^2 + \dot{z}^2$ represents wind energy staming from cyclonic activity. The depth of the mixing layer, and consequently the carrying capacity, are assumed to increase linearly with E in our model, with a small coupling constant. The most general form of the carrying capacity K is thus

$$K(t) = 1 - \alpha[\beta(c(t) - 1) - D_0 t + A \sin(\omega t)] + \gamma(\dot{x}^2 + \dot{y}^2 + \dot{z}^2). \tag{9}$$

Here $0 \leq \gamma \leq 0.2$ is the strength of a weak coupling c) due to oceanic mixing what we call the (oceanic) *mixing parameter*. This provides a feedback between the phytoplankton dynamics and the climatic variables.

3 Analytic results without mixing

Without mixing ($\gamma = 0$), Eq. (2) can be solved by a simple ansatz of $c(t)$, irrespective of the atmospheric dynamics. This leads to analytic results concerning some properties of the model, which are summarized in Supplementary Material I. As an example, we give here two simple relations which help to understand the general tendencies of the system. Eq. (2) with (9) is shown for $\gamma = 0$ to possess linear behavior for long times, inherited from the temperature contrast of anthropogenic origin:

$$c(t) \sim St, \quad F(t) \sim -Dt. \tag{10}$$

The linear coefficient, slope S in the phytoplankton concentration's time dependence is found to be

$$S = \frac{D_0 \alpha}{1 + \beta \alpha} \approx D_0 \alpha. \tag{11}$$

The approximate equality reflects that the product $\alpha \cdot \beta$ is quadratically small since both the enrichment parameter α and the extraction parameter β are small quantities. Hence the leading order behavior in α is linear. This relation shows that for

a positive (negative) coupling α the phytoplankton concentration increases (decreases) proportionally with the enrichment parameter α, and with the slope D_0 of the anthropogenic temperature contrast.

The linear coefficient in the temperature contrast is

$$D = \frac{D_0}{1 + \beta\alpha} \approx D_0(1 - \beta\alpha). \tag{12}$$

The approximate equality provides, again, the leading order behavior in α. The relation indicates that in the case of a positive enrichment parameter α the phytoplankton dynamics *weakens* the climate change, weakens the trend from D_0 to D in the temperature contrast, as expected. Quite surprisingly, however, the effect is rather weak since $\alpha \cdot \beta$ is quadratically small. Relations (11,12) also suggest that the role of (a weak) extraction coupling is not essential: the leading behavior in S is independent of β. Its effect is weak also in D, this quantity coincides with the anthropogenic slope D_0 for $\beta = 0$ (as also follows from (4)), it deviates from D_0 very little otherwise.

It is worth noting that relations (11,12) remain valid for the time-averaged trends in the presence of a seasonal periodicity, as also shown in Supplementary Material I. Relations (11,12) are independent of initial conditions, they represent the snapshot attractor of the problem projected on variable c. This attractor is fixed point-like, but changes in time (moves uniformly, or with an oscillation superimposed when seasonality is taken into account). There is, however, no internal variability in the concentration variable c, although an extended, fractal snapshot attractor underlies the atmospheric variables exactly as in the model of Drótos et al (2015) where no phytoplankton dynamics was taken into account.

4 Numerical results with mixing: trends in the fully coupled model

In the interesting case of nonnegligible mixing, no analytic result can be obtained. This implies a nontrivial biomass dynamics for $\gamma > 0$, a dynamics exhibiting internal variability in variable c, too. To explore this regime, we carried out a sequence of numerical simulations of the full 4-variable dynamics. The following parameters are kept fixed (as indicated in the previous section): $r = 1$, $D_0 = 2/7300$, $F_r = 9.5$, $A = 2$, $\omega = 2\pi/73$, and we vary α, β, and γ. Equations (1) and (2) with (4), (8) and (9) are solved with the classical 4th-order Runge-Kutta method with a fixed time-step $dt = 0.01 \approx 1.37 \times 10^{-4}$ y.

To start with, Fig. 1a shows a few individual concentration realizations (colored lines) $c(t)$ for a mixing parameter $\gamma = 0.1$ ($\alpha = 0.05$, $\beta = 0.1$), along with the ensemble average $<c>(t)$ of 50 000 realizations initiated at $t = -20$ y (purple line). The individual cases are all rather different. For $t < 0$ there is no climate change, nevertheless, the individual time series exhibit strong variance, very similar to those observed for $t > 0$, i.e., they are unable to properly reflect the ensemble, and, in particular, the lack of climate change for $t < 0$. The ensemble average, however, provides a plateau here up to $t = 0$ indicating clearly the stationarity of the climate and, therefore, of the biomass dynamics in this range. In Fig. 1b we display the source of the time variability of the phytoplankton concentration, the total kinetic energy $\dot{x}^2 + \dot{y}^2 + \dot{z}^2$ of the atmosphere at each time instant. The deviation of the individual ensemble member time series from the average is represented here by means of the standard deviation evaluated over the ensemble (violet bars). The average kinetic energy, along with its ensemble variance, is also constant before the climate change and starts an irregular time dependence right after $t = 0$. One can observe that the kinetic

energy strongly influences the phytoplankton concentration (via the carrying capacity K in (9)), but the concentration itself contributes to the CO_2 content, and to the temperature contrast F, see (4), forcing the atmosphere (as will be demonstrated in Fig. 2). The feedback of the atmosphere on phytoplankton is rather strong in this set-up with $\gamma = 0.1$, also expressed by the

210 strong difference between the green line (obtained for $\gamma = 0$) and the purple line in Fig. 1a illustrating that this coupling leads to an enormously enhanced biomass concentration.

It is visible in the inset to Fig. 1b that the ensemble average curve shows some change during the first 5 years (between $t = -20$ and -15 y). This indicates (along with several other simulations, not shown) that the convergence to the snapshot attractor takes about $t_c = 5$ y. The numerical data after $t = -15$ y thus represent parallel atmosphere-phytoplankton realizations

215 on the snapshot attractor of the system.

The considerable deviation of the individual time series from the ensemble average indicates that the formers are not representing properly the mean climate state, as also pointed out by Drótos et al (2015). Therefore, from here on, we shall concentrate on ensemble averages, and consider the variance about these as a measure of the internal variability (the size of the snapshot attractor in the chosen variable).

220 We carried out similar simulations with other extraction parameter values from the range $\beta \in [0.0, 0.5]$ and found that β does not have much effect on the average phytoplankton concentration, the curves for various values of β are close to each other (see Fig. S1 in Supplementary Material II). In what follows, therefore, we stick to a single value, $\beta = 0.1$.
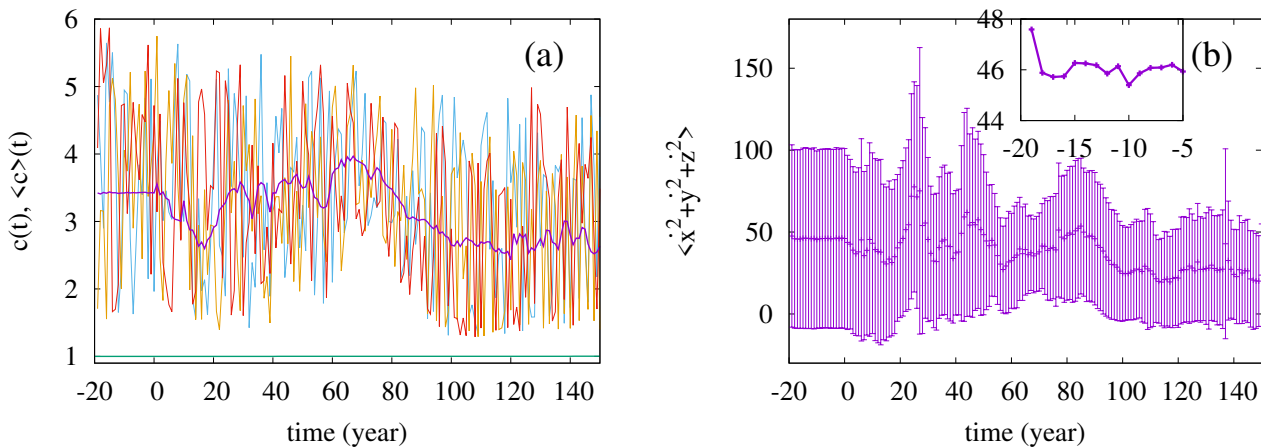
Figure 1. Ensemble properties before ($t < 0$) and after ($t > 0$) the onset of climate change. a) Phytoplankton concentration c as a function of time for three random initial conditions in different colors for $\alpha = 0.05$, $\beta = 0.1$, $\gamma = 0.1$. The purple line is the ensemble average $< c > (t)$ for 50000 trajectories started with random initial positions in the range $x \in [-0.5, 3]$, $y, z \in [-2.5, 2.5]$, $c \in [0.9, 1.1]$ at year -20. The green line (close to $c = 1$) shows the expected phytoplankton concentration without any mixing ($\gamma = 0$) as predicted by Eq. (10). (The increase for $t > 0$ is so weak that one hardly recognizes it on this graph.) b) Time-dependence of the ensemble average (dark violet "+" marks) of the total atmospheric kinetic energy $< \dot{x}^2 + \dot{y}^2 + \dot{z}^2 >$ for the same ensemble as the one used for c in (a). Violet bars indicate the standard deviation. The inset shows the blow up of the initial part of the average in b).

The time-dependence of the typical (ensemble averaged) temperature contrast $<F>(t)$ forcing the atmospheric variables in (1) is shown in Fig. 2. The value of $<F>(t)$ at each time instant is computed from Eqs. (4), (8), with the average values $\langle c \rangle$

225 (ensemble average over 50000 trajectories at that time instant) in place of c. The fluctuations in the $<F>(t) = F(<c>(t),t)$ curve of Fig. 2 follow the fluctuations in the average phytoplankton concentration, but, for small values of γ, the linear decrease of $F(t)$ is recovered. In other words, for weak mixing (small values of γ) the trend in the forcing $F(t)$ follows quite closely the direct anthropogenic trends. For strong mixing ($\gamma \leq 0.1$), however, the fluctuations have longer time-scale, hence the trends imposed by anthropogenic effects are less obvious, in particular, on shorter time-scales. A comparison of Figs. 2 a and b

230 belonging to $\alpha = 0.05$ and $\alpha = -0.05$, respectively indicates that a change in the sign of the enrichment parameter leads to only minor differences in the general trends.
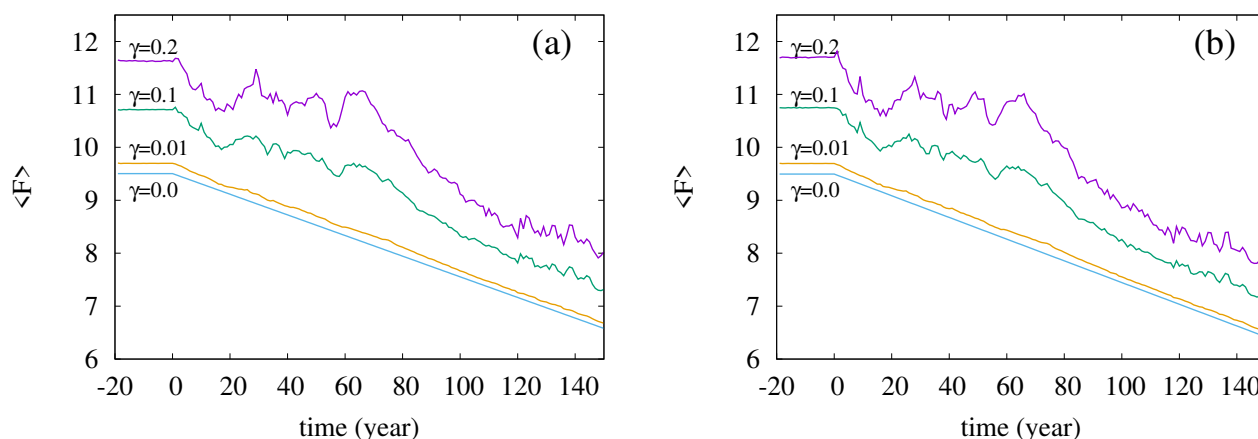
Figure 2. Time-dependence of the ensemble averaged atmospheric forcing $<F>(t) = F(<c>(t),t)$ in case of $\gamma = 0, 0.01, 0.1$ and 0.2 for a) $\alpha = 0.05$, b) $\alpha = -0.05$. The slope of the blue line for $\gamma = 0$ corresponds to D in (12).

Next, we study the dependence of the ensemble average of the phytoplankton concentration on the strength of mixing. We have seen in Fig. 1 that for $\gamma = 0.1$ strong deviations appear from the trend, αD_0, occurring without mixing. The time dependence of $<c>$ for mixing parameters on this order of magnitude, shown in Fig. S2 of Supplementary Material II,

235 confirms the existence of large fluctuations. The time dependence of $<c>$ for much smaller values of γ are shown in Fig. 3. The linearly increasing trend in harmony with (10) and (11) gradually disappears, and large scale fluctuations are visible even for $\gamma = 0.005$.

It seems that even a small coupling of the atmospheric variables x, y and z to the phytoplankton dynamics will result in large variations of $<c>$ and in the suppression of the anthropogenic trends on short terms. One can also conclude from these

240 figures that a coupling with $\gamma \geq 0.002$ should already be considered strong in the atmosphere-ocean interaction, at least from the point of view of the phytoplankton dynamics.

Now we investigate the effect of the enrichment parameter α on the phytoplankton concentration. We have seen in Fig. 3 that for small $\alpha = 0.05$, the short term trends are destroyed for $\gamma > 0.002$. We see in Fig. 4 that with an increase of $|\alpha|$, a trend
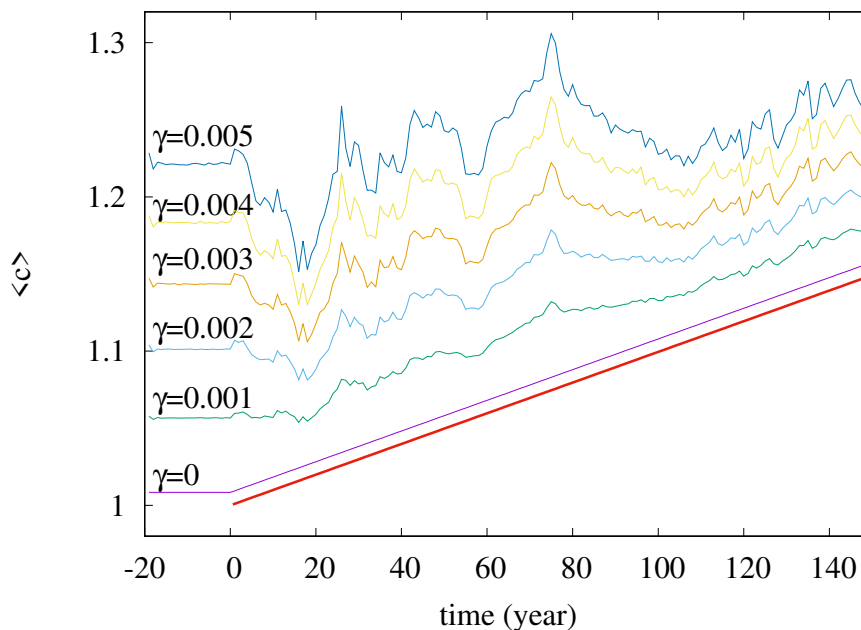
Figure 3. Ensemble averaged phytoplankton concentration $\langle c \rangle$ as a function of time for $\alpha = 0.05$ for various values of γ ($\gamma = 0, 0.001, 0.002, 0.003, 0.004$ and $\gamma = 0.005$). The thick red line shows the expected phytoplankton concentration in lack of mixing ($\gamma = 0$) as predicted by Eq. (11).

might reappear at even higher values of the mixing parameter $\gamma = 0.01$. Indeed, for α between roughly -0.05 and 0.05, no

245   trend is visible, large scale fluctuations stamming from the internal variablility of the dynamics rule the behavior of the average phytoplankton population. For $|\alpha| \geq 0.1$, however, we see that trends emerge, there is an increasing trend for positive, and a decreasing trend for negative α with a slope similar to the one given by the analytic calculation valid for $\gamma = 0$.

     From the same set of α values used to construct Fig. 4, we show the time-dependence of the average forcing $< F > (t)$ for an intermediate ($\gamma = 0.01$) and a large ($\gamma = 0.1$) mixing parameter in Fig. 5a and b, respectively. Interestingly, for each value

250   of α and γ, the $< F > (t)$ graphs show a nearly linear decay, the slope depending somewhat on α. It seems that the direct anthropogenic component is dominant in the average forcing term, in particular for $\gamma = 0.01$, but this also holds qualitatively for $\gamma = 0.1$ (see Fig. 5b). We thus conclude that a mixing parameter on the order of 0.1 is not yet strong from the point of view of the forcing. This is in harmony with the observation that the atmospheric kinetic energy hardly depends on the mixing strength (see Fig. S3 of Supplementary Material II): the atmosphere is rather resistant against the feedback from the

255   biomass. Although an increased (decreased) amount of phytoplankton present in the system results in an increased (decreased) temperature contrast and hence in a decreased (enhanced) climate change, this effect is quite small. The order of magnitude of the effect of the phytoplankton concentration on $< F > (t)$ can be assessed by observing in Fig. 4 that $(\langle c \rangle - 1)$ falls between -0.5 and 1 at $t = 150y$. Multiplied by our fixed $\beta = 0.1$, as (4) requires, one finds a range of 0.15, which is much smaller than
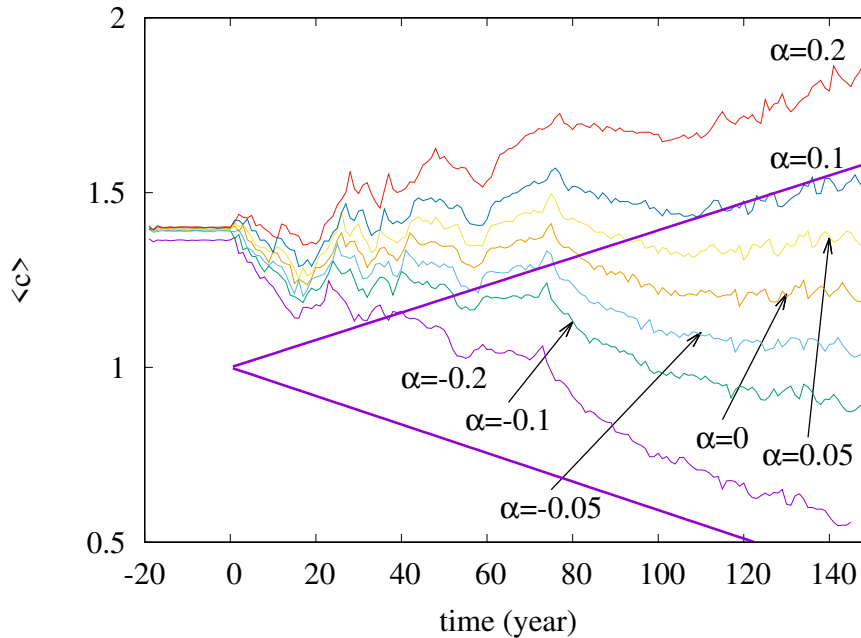
Figure 4. Average phytoplankton concentration $\langle c \rangle$ as a function of time for $\gamma = 0.01$ for various values of α (-0.2, -0.1, -0.05, 0.0, 0.05, 0.1 and 0.2). The thick purple lines show the expected phytoplankton concentration without mixing ($\gamma = 0$) as predicted by Eq. (11) for $\alpha = -0.2$ (lower line) and $\alpha = 0.2$ (upper line).

the final value of F, about 7, at 150 y. This is comparable with the spread of the temperature contrast at the end of year 150

260   in Fig. 5a and b. Note that these conclusions are drawn from the average temperature contrast. No trend can be extracted if instantaneous values of a single simulation are used instead of the ensemble average, in the same spirit as in Fig. 1a.

Next, we study quantitavely how the trend observed in the ensemble average of the phytoplankton concentration changes with the parameters. To this end, we fit a straight line to the time dependence of the ensemble average $\langle c \rangle(t)$ of the phytoplankton concentration for $t > 0$ for various values of parameters α and γ. The slope $S(\alpha, \gamma)$ of the best fit line in the presence of mixing

265   gives information on the trend of the phytoplankton concentration, that is, on how quickly the concentration changes with time on (ensemble) average. We have also computed the standard deviations of this fit from the measured values to gain information on the fluctuations appearing in individual members of the ensemble. We found (not shown) that in case of a strong trend (slope of time-dependence far from zero) we find small fluctuations and vice versa.

In Fig. 6 we show the approximate slope $S(\alpha, \gamma)$ of the $\langle c \rangle(t)$ curves as a function of the mixing parameter γ. We see

270   that the measured slopes, that is, the trends in the time-dependence, decrease with increasing values of γ. We also found that the fluctuations (not shown) are enhanced when γ increases. This implies that when mixing becomes stronger, not only the phytoplankton concentration is decreasing for any α (the slope is negative), but even drops faster (the slope is decreasing). Note that the initial concentration from which the decrease starts at $t = 0$ is higher for larger γ (stronger mixing), see Fig. 3
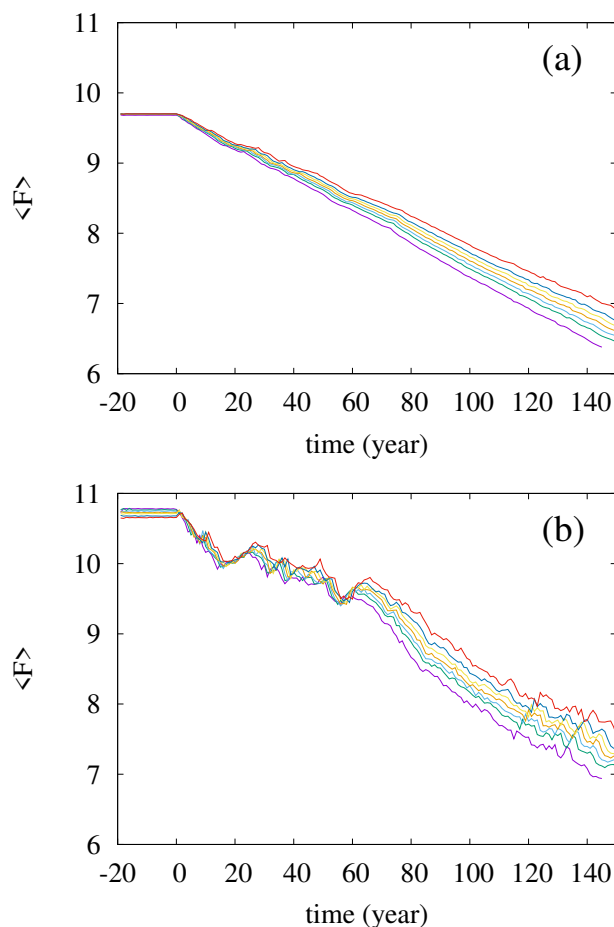
Figure 5. Time dependence of the average forcing $< F > (t)$ in case of (a) $\gamma = 0.01$ and (b) $\gamma = 0.1$. The values of the enrichment parameter from top to bottom are $\alpha = 0.2, 0.1, 0.05, 0, -0.05, -0.1$ and -0.2.

and Fig. S2 of Supplementary Material II. Concerning the fluctuations, we call the attention to the fact that in nearly all
275 figures exhibiting time dependence one can observe a decrease in the amplitude of variations for longer times, for $t > 100y$
approximately. This appears to be a consequence of the decrease of the total atmospheric kinetic energy with time, due to the
overall decrease of the temperature contrast in time, as Fig. S3 of Supplementary Material II. also illustrates. At a fixed mixing
parameter γ, the strength of mixing is proportional to the kinetic energy, which is thus decreasing in time. Since the carrying
capacity is assumed to linearly depend on the kinetic energy (see (9)), K also decreases in time. Thus, the phytoplankton
280 concentration and its fluctuations are also decreasing with time.

It is worth also noting that even if for $\gamma = 0$ the trend in $< c >$ would be increasing for positive enrichment parameters, see
(11), it is the increase of γ that converts all trends to be negative. It remains true, however, that the trend for a positive α is less
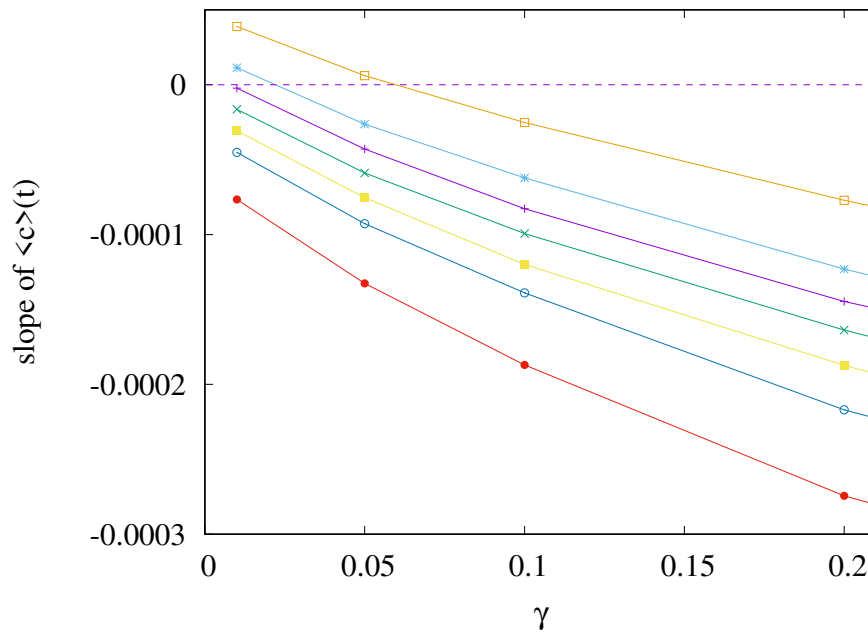
Figure 6. Slope S of the ensemble average of the phytoplankton concentration, $< c >$, for $t > 0$ as γ is varied, data shown for various values of α, from top to bottom, $\alpha = 0.2, 0.1, 0.05, 0, -0.05, -0.1$ and -0.2.

negative than for a negative α. In other words, for sufficiently strong mixing, the phytoplankton concentration always decreases with time due to climate change, the sign of the enrichment parameter only influences the strength of decrease.

285   If we plot the same data shown in Fig. 6 as a function of α instead of γ, see Fig. 7a, we see that the increase in the enrichment parameter increases the trend in the phytoplankton concentration. It is a surprising observation that even if the change in the mixing parameter changes the slopes essentially, their α-dependence remains similarly linear as for $\gamma = 0$ given in (11). Plotting the slope $-D(\alpha, \gamma)$ of the time-dependent ensemble averaged forcing $< F >$ as a function of α, see Fig. 7b, a very weak dependence is found (note the vertical scale). On a closer look, the α-dependence is linear, and is increasing. This

290   is in harmony with the expectation that the CO_2 extraction is weaker when the phytoplankton concentration is lower. With the exception of small γ values, the slopes are more negative than the direct anthropogenic one, $-D_0$. It is a remarkable finding suported by our results that a large mixing parameter enhances the speed of the climate change, irrespective of the sign of the enrichment parameter.

We see that the trends predicted by Eqs. (11,12) are approached when γ is decreased. What is even more interesting, the

295   dependence of the trends on α remains the same for any γ. In particular, we find a numerical fit of the slope S of $< c > (t)$ for $\beta = 0.1$ as

$$S(\alpha, \gamma) = \alpha D_0 (1 + 3.8\gamma) - 2D_0 \gamma^{0.75}. \tag{13}$$
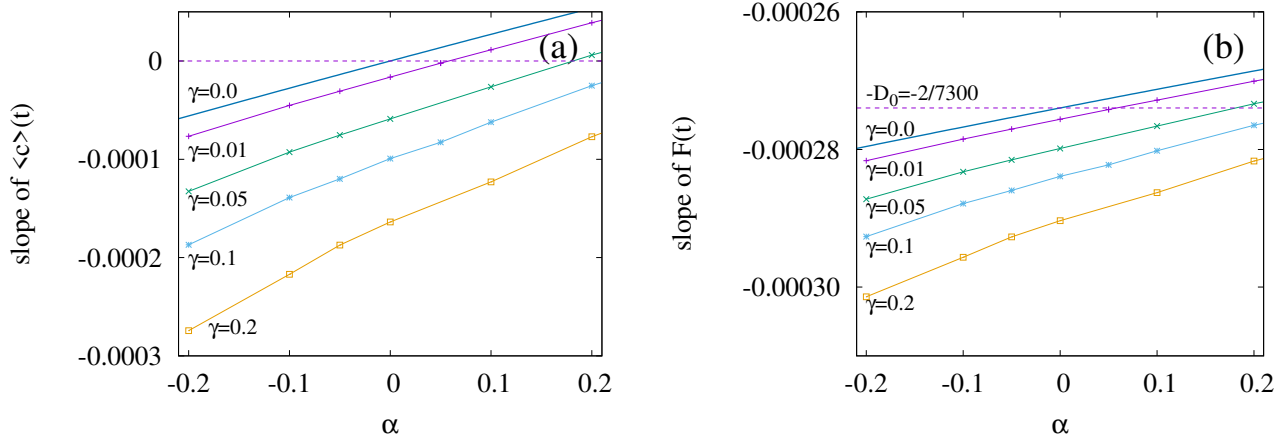
Figure 7. Slope (a) S of the ensemble averaged phytoplankton concentration $<c>(t)$ and (b) $-D$ of the average forcing $<F>$ for $t>0$ as α is varied, data shown for various values of γ. The $\gamma=0$ curve shows the α-dependence of (a) S and (b) $-D$ from Eqs. (11,12). Dashed lines mark the slopes for $\alpha=0, \gamma=0$.

A similar expression is obtained from the slopes of the averaged forcing $<F>(t)$ that replaces D_0 found in (12) for $\gamma=0$ by

$$D(\alpha,\gamma) = D_0[1-\alpha\beta(1+3.8\gamma)] + 2\beta D_0\gamma^{0.75}. \tag{14}$$

300 It is surprising that the leading order linear behavior in the enrichment parameter α found for S and D without any mixing remains valid for practically the entire γ range investigated, just the coefficients become γ-dependent.

5 Snapshot attractors

For several parameter values, we also determined the snapshot attractors of the coupled model. An example is given in Fig. 8 where we see the attractor on the $z=0$ slice of the atmospheric dynamics with the corresponding c-values not shown directly.
305 Different colors indicate different time instances separated by 10 y, clearly indicating that the attractor is changing in time. As the colors indicate, the projection to the (x,y) plane of the $z=0$ cross-section of the snapshot attractor has a minimum size in years 60–80, after which it increases again, and the maximum extension is reached by about year 150. Note that one cannot decide how much of the time dependence is a consequence of $F_0(t)$ or of the phytoplankton concentration. Due to the couplings between the biomass and the atmosphere, the direct anthropogenic effect cannot be separated from the effect of the
310 biomass.

By investigating a projection of the snapshot attractor on a plane containing concentration c as one of the axes, the influence of mixing on the internal variability within c can be visualized. In Fig. 9, the $z=0$ slice of the snapshot attractor of a given time instant is shown for three values of γ, projected to the x,c plane, that is, the y values are not shown. We see that the extension of the snapshot attractor in the c direction is greatly affected by the strength of mixing: the c extension is zero for $\gamma=0$, but
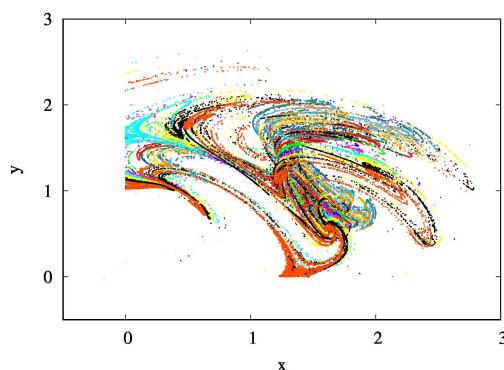
Figure 8. The projection of the $z = 0$, $\dot{z} > 0$ section of the snapshot attractors on the x, y plane for $\beta = 0.1$, $\alpha = 0.05$, $\gamma = 0.1$. The snapshot attractors at intervals of 10 years are shown with purple ($t = -10$ y), green ($t = 0$ y), cyan ($t = 10$ y), light orange (($t = 20$ y), yellow ($t = 30$ y), dark cyan ($t = 40$ y), dark red ($t = 50$ y), dark grey ($t = 60$ y), grey ($t = 70$ y), red ($t = 80$ y), light green ($t = 90$ y), blue ($t = 100$ y), pink ($t = 110$ y), light blue ($t = 120$ y), bright yellow ($t = 130$ y), black ($t = 140$ y), dark orange ($t = 150$ y). They are generated by initiating 7×10^7 random initial conditions at year -20.
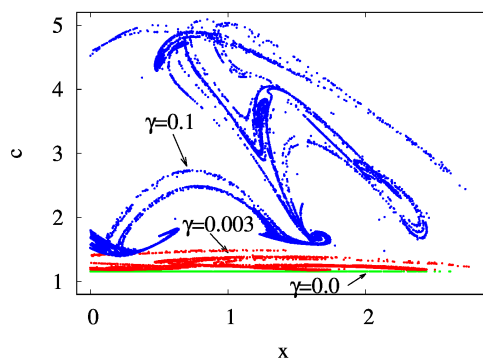
Figure 9. The projection of the $z = 0$, $\dot{z} > 0$ section of the snapshot attractors at year 150 on the x, c plane for $\beta = 0.1$, $\alpha = 0.05$, and for $\gamma = 0.0$ (green), 0.003 (red) and 0.1 (blue).

315   increases rapidly for increasing γ. Parallel to this, the pattern becomes interwoven in the space of variables, suggesting that the c-dynamics becomes more and more complex in time, too. It is the increasing size and complexity of the snapshot attractor in the c direction which is reflected in the increase of the strength of fluctuations in Fig. 3 and Fig. S2 of Supplementary Material II.

      We also investigated the extremes of the snapshot attractors. That is, at a fixed time instant, we looked for those values of

320   e.g. x, for which only 10 % of values can be found on the snapshot attractor below (lower extreme) or above (higher extreme) x. These values of x are shown in Fig. 10a as a function of time. The interval between these thresholds is a measure of the size of the extension of the snapshot attractor at a given time instant. Clearly, this size undergoes strong variations as a function of
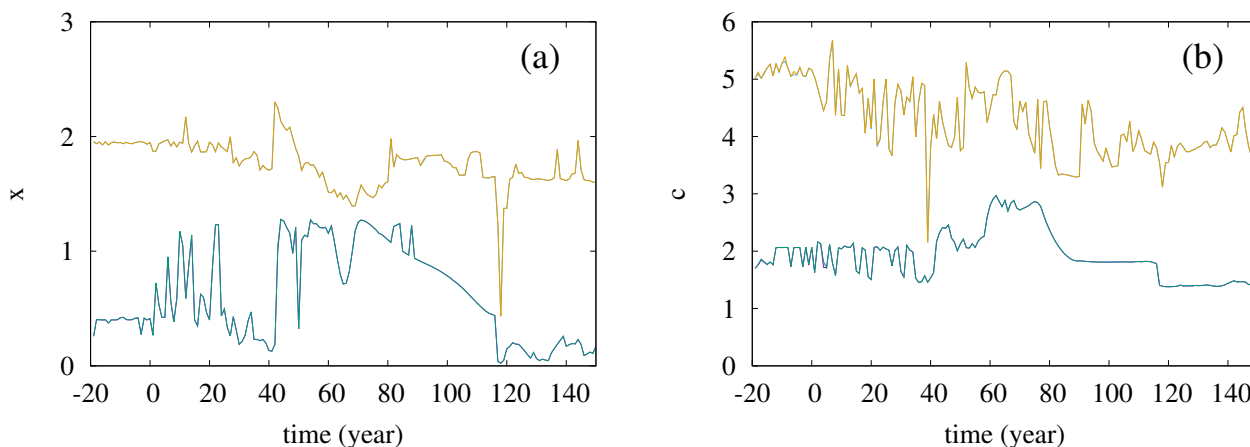
Figure 10. The extremes of the snapshot attractor for $\alpha = 0.05$, $\beta = 0.1$, $\gamma = 0.1$, Only 10 % of the points are found above (below) the higher (lower) values for each time instant for (a) x and (b) c.

time. The same is shown in Fig. 10b for the time dependence of the c extension of the snapshot attractor: the upper (lower) curve shows the value of c above (below) which only 10 % of the values appear on the snapshot attractor. Again, we see

325 considerable variations in time. It is interesting to note that, as these figures indicate, there is no unique trend in the size of the snapshot attractors, although trends can be seen in averages taken with respect to the ensemble designating the attractor itself, like e.g. in $< c >$ or $< F >$.

6 Conclusions

We have set up a conceptual coupled atmosphere–phytoplankton model by combining the Lorenz'84 general circulation model

330 and the logistic equation under the condition of a climate change due to a linear decrease in the strength of direct anthropogenic forcing. The novel features of the model are in the choice of the possible forms of couplings. We allow for an influence of the biomass on the atmospheric forcing, modeling this way the extractions of CO_2 by phytoplankton, but the same forcing is able to modify the carrying capacity via its coupling to the temperature contrast characterized by the enrichment parameter. An additional atmosphere-ocean coupling is also taken into account mimicking the enhancement of phytoplankton primary

335 production via increased atmospheric activity, i.e., via turbulent mixing. Our intention has been to include leading order effects, and hence the couplig constants are chosen intentionally to be small. Nevertheless, interesting consequences are found.

 By investigating the parameter dependence of the ensemble average of the atmospheric forcing and the phytoplankton content, we have shown that

  – even without mixing, the phytoplankton biomass interacts with the atmospheric forcing, and the coupling between the

340 phytoplankton concentration and the temperature might weaken or strengthen the anthropogenic warming trend, the

increase or decrease of the phytoplankton biomass depends on the sign of the enrichment parameter. In this regime, analytic results are available, see Eqs. (10, 11 and 12).

- increased mixing parameter enhances the total phytoplankton population biomass. Stronger coupling may enhance fluctuation to a degree that the anthropogenic component practically disappears (Fig. 3 and Fig. S2 of Supplementary Material II.).

- in contrast, mixing appears to depress the trend of the extraction of CO_2 by phytoplankton, and may force the phytoplankton population to globally decrease in time (see Fig. 6), although starting from a higher initial level.

- the coupling of mixing with phytoplankton biomass has a much weaker effect on the atmospheric forcing (see Fig. 5), as it is minimally expected from a coupled atmosphere-phytoplankton model.

- despite the strong modifications due to mixing, the dependence of trends on the strength of the coupling between the phytoplankton concentration and the temperature (the enrichment parameter) remains practically the same as without mixing (see Fig. 7).

We have obtained these results in a conceptual coupled atmosphere–phytoplankton model which contains a tractable number of variables and parameters. To our knowledge, this is the first attempt to understand the general and robust features of the interplay between the atmosphere and the biosphere in a climate change framework. We expect that our paper gives guidance to targeted numerical studies of Earth System Models as well as an example for theoretical analysis of coupling between biogeochemisty and climate.

Author contributions. T. Tél worked out the outline of the applied model, I. Scheuring contributed the biological details, Gy. Károlyi developed the simulation code, Gy. Károlyi and R.D. Prokaj carried out the simulations, all authors contributed to the preparation of the manuscript.

Competing interests. The authors declare that they have no conflict of interest.

Acknowledgements. We are thankful for the useful comments to T. Bódai, G. Drótos and T. Haszpra. This work was supported by the National Research, Development and Innovation Office of Hungary under grant K-125171. IS is supported by Hungary's Economic Development and Innovation Operative Program (GINOP 2.3.2-15-2016-00057). GyK is supported by grant BME FIKP-VÍZ of EMMI.

365 **References**

Basu, S., K.R.M Mackey, 2018: Phytoplankton as Key Mediators of the iological Carbon Pump: Their Responses to a Changing Climate. *Sustainability*, **10**, 869.

Blunden, J., and D.S. Arndt, 2013: State of the climate in 2012. *Bull. Amer. Meteor. Soc.*, **94**, S1–S258.

Bódai, T., G. Károlyi, and T. Tél, 2011: A chaotically driven model climate: extreme events and snapshot attractors. *Nonlin. Processes*
370 *Geophys.*, **18**, 573-580.

Bódai, T., G. Károlyi, and T. Tél, 2013: Driving a conceptual model climate by different processes: Snapshot attractors and extreme events. *Phys. Rev. E*, **87**, 022822, 1-10.

Bódai, T. and T. Tél, 2012: Annual variability in a conceptual climate model: Snapshot attractors, hysteresis in extreme events, and climate sensitivity. *Chaos*, **22**, 023110, 1-11.

375 Chekroun, M.D., E. Simonnet, and M. Ghil, 2011: Stochastic climate dynamics: Random attractors and time-dependent invariant measures. *Physica D*, **240**, 1685-1700.

Chust, G., et al, 2014: Biomass changes and trophic amplification of plankton in a warmer ocean. *Global Change Biology*, **20** 2124-2139, doi: 10.1111/gcb.12562.

De La Rocha, CL., and U. Passow, 2014: The Biological Pump, in: Turekian, K.K., Holland, H.D. (Eds.): Treatise on Geochemistry. *(Else-*
380 *vier)*, **8**, 93-122, https://doi.org/10.1016/B978-0-08-095975-7.00604-5.

Drótos, G., T. Bódai, and T. Tél, 2015: Probabilistic concepts in a changing climate: A snapshot attractor picture. *Journal of Climate*, **28**, 3275-3288.

Drótos G., T. Bódai, and T. Tél, 2017: On the importance of the convergence to climate attractors, Eur. Phys. J. Special Topics **226**, 2031-2038

Estrada, M., and E. Berdalet, 1997: Phytoplankton in a turbulent world. *Scientia Marina*, **61**, 125-140.

385 Falkowski, P.G., 2014: Biogeochemistry of Primary Production in the Sea in: Turekian, K.K., Holland, H.D. (Eds.): Treatise on Geochemistry. *(Elsevier)*, **10**, 163-187, https://doi.org/10.1016/B978-0-08-095975-7.00805-6.

Falkowski, P.G., R.T. Barber, and V. Smetacek, 1998: Biogeochemical controls and feedbacks on ocean primary production. *Science*, **281**, 200-206.

Falkowski, P.G., E.A. Laws, R.T. Barber, and J.W. Murray, 2003: Phytoplankton and their role in primary, new, and export production. In:
390 Fasham, M.J.R. (Ed): Ocean Biogeochemistry. Global Change – The IGBP Series. Springer, Berlin, Heidelberg

Falkowski, P., R.J. Scholes, E. Boyle, J. Canadell, D. Canfield, J. Elser, N. Gruber, K. Hibbard, P. Hogberg, S. Linder, et al., 2000: The global carbon cycle: A test of our knowledge of Earth as a system. *Science*, **290**, 291–296.

Ghil, M., M.D. Chekroun, and E. Simonnet, 2008: Climate dynamics and fluid mechanics: Natural variability and related uncertainties. *Physica D*, **237**, 2111-2126.

395 Guidi, L., S. Chaffron, L. Bittner, D. Eveillard, A. Larhlimi, S. Roux, and G. Gorsky, 2016: Plankton networks driving carbon export in the oligotrophic ocean. *Nature*, **532**, 465-470, https://doi.org/10.1038/nature16942.

Hader, D.P., V.E. Villafane, E.W. Helbling, 2014: Productivity of aquatic +primary producers under global climate change. *Photochem. Photobiol. Sci.*, **13**, 1370–1392.

Haszpra, T, M. Herein, 2019: Ensemble-based analysis of the pollutant spreading intensity induced by climate change. *Scientific Reports*, **9**,
400 3896.

Haszpra T., D. Topal, M. Herein, 2019: On the time evolution of the Arctic Oscillation and the related wintertime teleconnections under different forcing scenarios in an ensemble approach, preprint

Herein, M., G. Drótos, T. Bódai, F. Lunkeit, and V. Lucarini, 2019: Reconsidering the relationship of the El Niño–Southern Oscillation and the Indian monsoon using ensembles instate-of-the-art Earth system models. *Preprint*.

405   Herein, M., G. Drótos, T. Haszpra, J. Marfy, and T. Tél, 2017: The theory of parallel climate realizations as a new framework for teleconnection analysis. *Sci. Rep.*, **7**, 44529.

Hutchins, D.A., F Fu, 2017: Microorganisms and ocean global change. *Nat. Microbiol.*, **2**, 17058.

Jäger, C.G., S. Diehl, and M. Emans, 2010: Physical Determinants of Phytoplankton Production, Algal Stoichiometry, and Vertical Nutrient Fluxes. *the American Naturalist*, **175**, 4, E91-E104.

410   Kaszás, B., T. Haszpra, M. Herein, 2019: The snowball Earth transition in a climate model with drifting parameters: Splitting of the snapshot attractor. *Chaos*, **29**, 113102.

Li, W., K.S. Gao, J. Beardall, 2012: Interactive effects of ocean acidification and nitrogen-limitation on the diatom phaeodactylum tricornutum. *PLoS ONE*, **7**, e51590.

Lorenz, E.N., 1984: Irregularity: A fundamental property of the atmosphere. *Tellus*, **36A**, 98-110, doi:10.1111/ j.1600-0870.1984.tb00230.x.

415   Lorenz, E.N., 1990: Can chaos and intransitivity lead to interannual variability? *Tellus*, **42A**, 378-389, doi:10.1034/j.1600-0870.1990.t01-2-00005.x.

Mackey, K.R.M., J.J. Morris, F.M.M. Morel, and S.A. Kranz, 2015: Response of Photosynthesis to Ocean Acidification. *Oceanography*, **28**, 2, 74-91, https://doi.org/10.5670/oceanog.2015.33.

Marinov, I., S.C. Doney, and I.D. Lima, 2010: Response of ocean phytoplankton community structure to climate change over the 21st century:
420   partitioning the effects of nutrients, temperature and light. *Biogeosciences*, **7**, 3941-3959, https://doi.org/10.5194/bg-7-3941-2010.

Mongwe, N.P., M. Vichi, and P.M.S. Monteiro, 2018: The seasonal cycle of pCO2 and CO2 fluxes in the Southern Ocean: diagnosing anomalies in CMIP5 Earth system models. *Biogeosciences*, **15**, 2851–2872, https://doi.org/10.5194/bg-15-2851-2018.

Peters, F., and C. Marrasé, 2000: Effects of turbulence on plankton: an overview of experimental evidence and some theoretical considerations. *Mar. Ecol. Prog. Ser.*, **205**, 291-306.

425   Pierini, S., M.D. Chekroun, M. Ghil, 2018: The onset of chaos in nonautonomous dissipative dynamical systems: a low-order ocean-model case study. *Nonlinear Processes in Geophysics*, **25**, 671.

Pierini, S., M. Ghil, and M.D. Chekroun, 2016: Exploring the pullback attractors of a low-order quasigeostrophic ocean model: The deterministic case. *J. Clim.*, **29**, 4185-4202.

Reid, P.C., et al, 2009: Chapter 1. Impacts of the oceans on climate change. *Adv Mar Biol.*, **56**, 1-150, doi: 10.1016/S0065-2881(09)56001-4.

430   Roberts, C.M., et al, 2017: *Marine reserves can mitigate and promote adaptation to climate change PNAS*, **114**, 24, 6167-6175, https://doi.org/10.1073/pnas.1701262114.

Romeiras, F.J., C. Grebogi, and E. Ott, 1990: Multifractal properties of snapshot attractors of random maps. *Phys. Rev. A*, **41**, 784-799.

Sanders, R., S.A. Henson, M Koski, C.L. De la Rocha, S.C. Painter, A.J. Poulton, J. Riley, B. Salihoglu, A. Visser, A. Yool, et al., 2014: The biological carbon pump in the north Atlantic. *Prog. Oceanogr.*, **129**, 200–218.

435   Schlunegger, S., K.B. Rodgers, J.L. Sarmiento, T.L. Frölicher, J.P. Dunne, M. Ishii, R. Slater, 2019: Emergence of anthropogenic signals in the ocean carbon cycle. *Natue Climate Change*, **9**, 719-725.

Serezze, M.C., and J.A. Francis, 2006: The Arctic amplification debate. *Climate Change*, **76**, 241.

Stocker, T.F. and Coauthors, 2013: The Physical Science Basis. Contribution of Working Group I to the Fifth Assessment Report of the Intergovernmental Panel on Climate Change. (Cambridge University Press, Cambridge,and New York, 2013)

440 Sverdrup, H.U., 1953: On conditions for the vernal blooming of phytoplankton. *Journal du Conseil International pour l'Exploraton de la Mer*, **18**, 287-295.

Turner, J.T. 2015: Zooplankton fecal pellets, marine snow, phytodetritus and the ocean's biological pump. *Prog. Oceanogr.*, **130**, 205–248.

Vincze, M., 2016: Modeling climate change in the laboratory, in Teaching Physics Innovatively. *pp*, 107-118. edited by A. Kiraly and T. Tel (Ph.D. School of Physics, Eotvos University, Budapest, 2016), pp. 107–118.

445 Vincze, M., I.D. Borcia, and U. Harlander, 2017: Temperature fluctuations in a changing climate: an ensemble-based experimental approach. *Sci. Rep.*, **7**, 254.

Whitt D.B., J.R. Taylor, and M. Levy, 2017: Synoptic-to-planetary scale wind variability enhances phytoplankton biomass at ocean fronts. *Journal of Geophysical Research: Oceans*, **122**, 4602-4633, DOI:10.1002/2016JC011899.

Wilson, J.D., F.M. Monteiro, D.N. Schmidt, B.A. Ward, and A. Ridgwell, 2018: Linking Marine Plankton Ecosystems and Cli-
450 mate: A New Modeling Approach to theWarm Early Eocene Climate. *Paleoceanography and Paleoclimatology*, **33**, 1439-1452, https://doi.org/10.1029/2018PA003374.

Zhong, Y., Z. Liu, and M. Notaro, 2011: A GEFA Assessment of Observed Global Ocean Influence on U.S. Precipitation Variability: Attribution to Regional SST Variability Modes. *Journal of Climate*, **24**, 3, 693-707, https://doi.org/10.1175/2010JCLI3663.1.